





Magnetic field dependent cycloidal rotation in pristine and Ge-doped CoCr_2O_4

N. Ortiz Hernández ^{1,*}, S. Parchenko^{1,*}, J. R. L. Mardegan^{1,4}, M. Porer¹, E. Schierle², E. Weschke², M. Ramakrishnan ¹, M. Radovic¹, J. A. Heuver³, B. Noheda³, N. Daffé¹, J. Dreiser¹, H. Ueda ¹ and U. Staub ^{1,‡}

¹Swiss Light Source, Paul Scherrer Institute, Forschungsstrasse 111, 5232 Villigen PSI, Switzerland

²Helmholtz-Zentrum Berlin für Materialien und Energie GmbH, Albert-Einstein-Strasse 15, 12489 Berlin, Germany

³Zernike Institute for Advanced Materials, University of Groningen, Nijenborgh 4, 9747AG, The Netherlands

⁴Deutsches Elektronen-Synchrotron, Notkestrasse 85, 22607 Hamburg, Germany



(Received 9 October 2020; revised 28 January 2021; accepted 1 February 2021; published 16 February 2021)

We report a soft x-ray resonant magnetic scattering study of the spin configuration in multiferroic thin films of $\text{Co}_{0.975}\text{Ge}_{0.025}\text{Cr}_2\text{O}_4$ (Ge-CCO) and CoCr_2O_4 (CCO) under low and high magnetic fields from 0.2 to 6.5 T. A characterization of Ge-CCO at a low magnetic field was performed, and the results were compared with those of pure CCO. The ferrimagnetic phase transition temperature $T_C \approx 95$ K and the multiferroic transition temperature $T_S \approx 27$ K in Ge-CCO are comparable with those observed in CCO. In Ge-CCO, the ordering wave vector ($qq0$) observed below T_S is slightly larger compared with that of CCO, and unlike CCO, the diffraction intensity consists of two contributions that show a dissimilar x-ray polarization dependence. In Ge-CCO, the coercive field observed at low temperatures was larger than the one reported for CCO. In both compounds, an unexpected reversal of the spiral helicity, and therefore the electric polarization, was observed on simply magnetic field cooling. In addition, we find a change in the helicity as a function of momentum transfer in the magnetic diffraction peak of Ge-CCO, indicative of the presence of multiple magnetic spirals.

DOI: [10.1103/PhysRevB.103.085123](https://doi.org/10.1103/PhysRevB.103.085123)

I. INTRODUCTION

Magnetoelectric (ME) multiferroics are of enormous interest from a technological perspective for designing functionalities such as using electric fields to manipulate magnetic order [1,2]. Of special interest are type II multiferroics, where magnetic ordering drives the electric polarization with both order parameters being strongly coupled. This strong coupling enables switching the polarization by a magnetic field or the magnetization by an electric field, which is energetically more efficient.

CoCr_2O_4 (CCO) is one of the few known ME multiferroics of type II that exhibits a net magnetization due to its ferrimagnetic state [3]. CCO crystallizes in a spinel structure (AB_2O_4), having cubic symmetry ($Fd\bar{3}m$) with a lattice constant of 8.33 Å [3] in bulk. The Co^{2+} ions sit on the tetrahedral coordinated A sites and Cr^{3+} on the octahedral coordinated B sites, subdivided into B1 and B2 sites. This material has been well characterized in both bulk [4–7] and thin film [8–12] forms. However, the very small electric polarization reported in bulk CCO makes it extremely challenging to measure it in thin film CCO. Three magnetic phases have been found below room temperatures for bulk. Below $T_C \approx 93$ K, where CCO becomes ferrimagnetically ordered [4]. In this phase, uncompensated magnetic sublattices of Co^{2+} and Cr^{3+} yield in a remanent net magnetization. Additionally,

a spiral short-range order is reported to coexist within the long-range ferrimagnetic order [13]. In fact, the two magnetic sublattices B1 and B2 couple antiferromagnetically to each other with different opening angles for the cone, resulting in a net magnetic moment that is antiparallel to sublattice A. This produces a net magnetization along the [001] direction. Below $T_S \approx 26$ K, CCO gets an additional long-range magnetic spiral component, represented by an incommensurate modulation wave vector ($qq0$), with $q \approx \frac{2}{3}$ reciprocal lattice units (r.l.u.). This transverse conical magnetic structure induces a ferroelectric polarization along the $[\bar{1}10]$ direction [4]. Around $T_F \approx 15$ K, yet another magnetic phase transition to a commensurate spiral phase has been reported [4–7], the occurrence of which remains controversial. Choi *et al.* [5] and Chang *et al.* [6] reported the occurrence of a commensurate wave vector ($\frac{2}{3}\frac{2}{3}0$) and two additional incommensurate satellites in bulk CCO, with the new incommensurability being along the [110] and $[\bar{1}\bar{1}0]$ directions. A more recent paper by Windsor *et al.* [8] reported a single incommensurate spiral below T_F in an epitaxially grown strained film. However, in their paper, the width of the observed magnetic diffraction peak might have been too large to resolve additional long wavelength satellites. It should be noted that, in the absence of electric polarization measurements in CCO thin film, the existence of the multiferroic phase is indicated by the appearance of the transverse conical magnetic structure modulated by ($qq0$). This magnetic structure induces electric polarization by antisymmetric exchange striction. Therefore, the polarization direction in CCO is directly related to the helicity of the spin spiral as given by Katsura *et al.* [14]: $P \propto \hat{e}_{ij} \times (S_i \times S_j)$, where $S_{i,j}$ is the corresponding spin of the neighboring sites i and j , and \hat{e}_{ij} is the unit vector connecting the two sites which

*These authors contributed equally to this work.

†Present address: Laboratory for Mesoscopic Systems, Department of Materials, ETH Zurich, 8093 Zurich, Switzerland.

‡Corresponding author: urs.staub@psi.ch

is parallel to the magnetic ordering wave vector $Q = (qq0)$. The above relation implies that reversing the spin spiral results in a reversal of polarization and vice versa. For this paper, the slight tetragonal distortion presented in the CCO and Ge-CCO thin films is induced by a tensile strain from the substrate. Consequently, the magnetic ordering vector Q and the polarization vector point out of plane and in plane, respectively.

In this paper, we examine the effect of doping a small fraction of nonmagnetic Ge on the long-range magnetic order in CCO, reporting a slightly larger $(qq0)$ modulation vector. We compare the magnetic properties of epitaxial films of Ge-doped CCO with pure CCO in the multiferroic phase, detecting a larger saturation and coercive field in Ge-CCO. We also explore the behavior of the magnetic spin spiral in these systems under high magnetic fields, finding a multispin-cycloidal scenario in Ge-CCO. Furthermore, an unexpected cycloidal helicity preference with magnetic field cooling is found, implying an electric polarization preference defined solely via the magnetic field direction in both systems (Ge-doped and pristine CCO). For this, we use resonant soft x-ray scattering (RSXS), an excellent technique to study complex magnetic structures. Recently, RSXS has been employed to investigate oxide materials, particularly multiferroics [15–21]. RSXS has the advantage of being element and orbital specific while probing long-range electronic ordering phenomena. Moreover, RSXS offers a high sensitivity in observing magnetic ordering schemes, even for small sample volumes [22–24].

II. EXPERIMENTS

Thin films of CCO and Ge-doped CCO were grown by pulsed laser deposition, monitored *in situ* by reflection high-energy electron diffraction. The CCO thin films were grown with a thickness of ~ 80 nm on [110]-oriented MgO substrates, and they are the same as used in a previous paper [8]. A more detailed description on the growth process can be found in Ref. [11]. The same growth parameters were employed for the Ge-doped CCO with 2.5% Ge doping, grown on [110]-oriented MgO substrates, resulting in $\text{Co}_{0.975}\text{Ge}_{0.025}\text{Cr}_2\text{O}_4$ (Ge-CCO) films with a thickness like CCO.

A. RSXS (reflectivity and diffraction) under low magnetic fields on Ge-CCO

X-ray magnetic circular dichroism (XMCD) in reflectivity mode and magnetic diffraction data have been collected at the Resonant Elastic Soft X-ray Scattering end station [25], at the X11MA beamline [26] of the Swiss Light Source (SLS). Intensities of reflected circularly polarized x-rays were collected at $\theta = 5^\circ$ incidence for photon energies around the $\text{Co } L_{2,3}$ edges to obtain the XMCD signal in reflection mode (see experimental layout in Fig. 1). For the magnetic diffraction experiment, q scans were performed at 780 eV ($\text{Co } L_3$ edge). Both circular and linear x-ray polarizations were used. Data were collected with an IRD AXUV100 photodiode, covered by a 400-nm-thick Al filter to suppress visible light and secondary electrons. The sample was field cooled (FC) in an external field of 0.2 T along the [001] direction from 300 to 8 K before data collection.

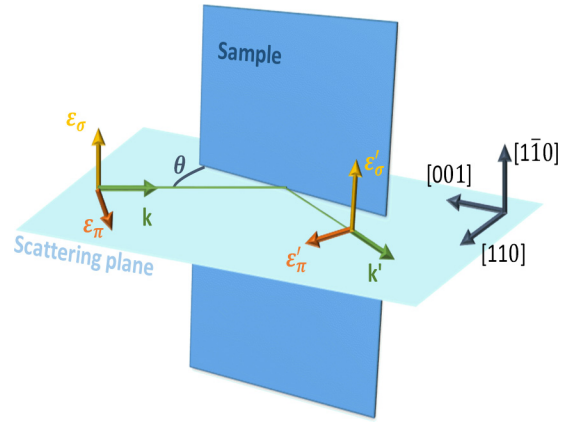


FIG. 1. Experimental geometry used in the Resonant Elastic Soft X-ray Scattering end station.

B. XMCD on Ge-CCO collected by x-ray excited optical luminescence

XMCD and magnetic hysteresis measurements were carried out at the X-Treme beamline [27] of the SLS using x-ray excited optical luminescence (XEOL) [8,28], taking advantage of the insulating character of the samples and the luminescence of the substrates. For luminescent substrates, XEOL effectively measures the absorption in transmission mode [29]. Hysteresis loops were collected at the energy with the largest XMCD around the $\text{Co } L_3$ edge (777.5 eV) for various temperatures. An incident angle of 30° with respect to [001] direction was chosen. The sample was FC from room temperature to 10 K in a field of -0.2 T along [001] (see Fig. 2).

C. RSXS on Ge-CCO and pure CCO under high magnetic fields

Resonant magnetic x-ray diffraction measurements at the $\text{Co } L_3$ absorption edge have been carried out on the high field diffractometer at the UE46_PGM1 beamline of BESSY II synchrotron, at Helmholtz Zentrum Berlin [30]. Incident linear and circular polarized x rays were used at energies around the $\text{Co } L_{2,3}$ edge. A dome was built with 400-nm-thick

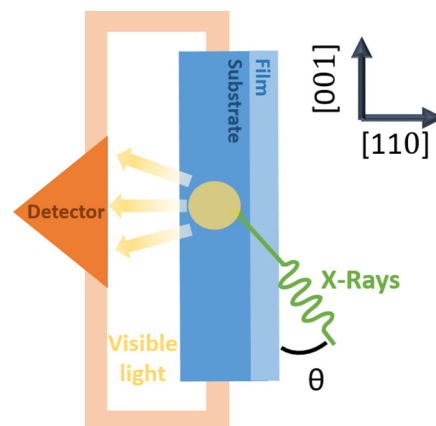


FIG. 2. Layout of x-ray excited optical luminescence (XEOL) experiment.

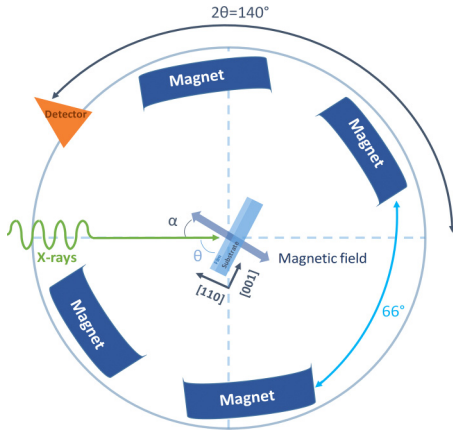


FIG. 3. Schematic representation of the experimental geometry. For $(qq0)$ reflection, the detector was placed at $2\theta = 140^\circ$ with an incident angle (θ) of 69.75° . The magnetic field during measurements was rotated by an angle $\alpha = 32.5^\circ$ from incoming x-ray beam.

Al foil (same used in Sec. II A) and placed above the sample to block visible light and secondary electrons. Both CCO and Ge-CCO samples were simultaneously mounted on the same holder to have the same experimental conditions. During FC, the magnetic field was applied along [001]. Since the magnets are not rotated during the scans, the magnetic field direction changes with respect to the surface during a scan.

Figure 3 displays a sketch of the experimental geometry. The magnetic field is created by an arrangement of superconducting magnet coils which is rotatable with respect to the sample. As the magnetic diffraction ($qq0$) peak requires a large scattering angle and the diffraction peak is very broad with a width of $\approx 45^\circ$ in total scattering angle 2θ , the magnets were rotated by $\alpha = 32.5^\circ$ with respect to the incident beam to have the best possible scattering geometry. When the magnetic field points toward the detector, secondary electrons are deflected by the field, resulting in an artificial increase of the signal that disappears in the absence of the magnetic field. To reduce this effect, the sample holder was charged for a few seconds by applying an electric field along the [110] direction. To suppress the specular reflectivity background in the magnetic diffraction signal, the θ angle was displaced 0.25° from the specular condition.

III. RESULTS

A. RSXS (reflectivity and diffraction) under low magnetic fields on Ge-CCO

RSXS provides an element-specific measure of the electronic state and magnetic configuration of ions in a material [31]. In the case of a transition metal ion such as Co^{2+} , electric dipole excitations at $L_{2,3}$ absorption edges directly probe electron transitions from the $2p$ core to the $3d$ valance states. Thus, the spectra are sensitive to the electronic configuration of the $3d$ states and its spin configuration in the presence of a core hole [32]. The resonant magnetic scattering amplitude for a single ion can be expressed in the electric dipole

approximation ($E1E1$) as [32,33]

$$f_{E1E1} \propto [(\hat{\epsilon}'^* \cdot \hat{\epsilon})F^0 - i\hat{m} \cdot (\hat{\epsilon}'^* \times \hat{\epsilon})F^1 + (\hat{\epsilon} \cdot \hat{m})(\hat{\epsilon}'^* \cdot \hat{m})F^2], \quad (1)$$

where $\hat{\epsilon}$ and $\hat{\epsilon}'$ refer to the incoming and outgoing photon polarizations, \hat{m} is the unit vector of the magnetic moments and the terms $F^{(n)}$ are scattering tensors of rank n , which depend strongly on energy. Scattered intensity is proportional to $|f_0 + f_{E1E1}|^2$, f_0 being the sum over the nonresonant amplitudes. For ferromagnetic order (e.g., solely the Co sublattice), only the second term in Eq. (1) depends on the circular x-ray polarization and, to first order, is proportional to the magnetic moment. Hence, the circular dichroism can be approximated as proportional to the magnetic moment. The circular dichroism is, therefore, large for small scattering angles when the sample is magnetized along the film plane, and this is in the scattering plane, as it is in our case.

Figure 4(a) shows the energy spectra of the reflected beam at the Co $L_{2,3}$ edges for incident circular right (C^+) and circular left (C^-) polarized light for Ge-CCO. A clear contrast is observed between the two spectra. Figure 4(b) shows the magnetic circular dichroism represented by the asymmetry defined as $A = \frac{I_{C^+} - I_{C^-}}{I_{C^+} + I_{C^-}}$. The dashed vertical line indicates the energy with maximal asymmetry, which is approximately 20% at 779.5 eV. Figure 4(c) presents the asymmetry at 779.5 eV as a function of temperature. The black dashed lines indicate $T_C \approx 95$ K, which is estimated by a linear fit (indicated by the pink dashed line) and implies that it is a second-order phase transition with a critical exponent $\beta \approx \frac{1}{2}$. Above T_C , the circular dichroism disappears, indicating the transition to the paramagnetic phase, like that reported for pure CCO [8]. This suggests that a small amount of Ge doping does not affect the magnetic transition temperature of the ferrimagnetic phase significantly.

Figure 5(a) displays the magnetic diffraction intensity of the ($qq0$) peak in Ge-CCO vs r.l.u. (bottom axis) and in total momentum transfer (Q) (top axis) for various temperatures. The peak maximum is at least 0.03 r.l.u. higher than pure CCO [8].

From a Gaussian fit in Fig. 5(a), we extract the temperature dependence of the integrated intensity [Fig. 5(b)], the modulation parameter q [Fig. 5(c)], and the correlation length [Fig. 5(d)] calculated as $\xi = \frac{2}{\text{FWHM}}$, where FWHM is the full width at half maximum. It should be noted that the correlation length is only a meaningful interpretation under the assumption that the peak is not a composite of several reflections, which is, however, unlikely to be the case, as shown later. Figure 5(b) shows that the static antiferromagnetic component appears around 27 K, suggesting that the material is in the multiferroic state below this temperature, akin to pure CCO. Figure 5(c) shows an increase of the modulation parameter q from 0.67 to 0.72 r.l.u. with reduction in temperature. We observe an increase of the correlation length with increasing temperature, which contrasts with pure CCO [8]. This increase is prominent around 18 K, close to T_F [4–7].

For comparison, we show in Fig. 6 the magnetic diffraction ($qq0$) peak for circular and linear polarization with their corresponding circular ($I_{C^+} - I_{C^-}$) and linear ($I_\pi - I_\sigma$)

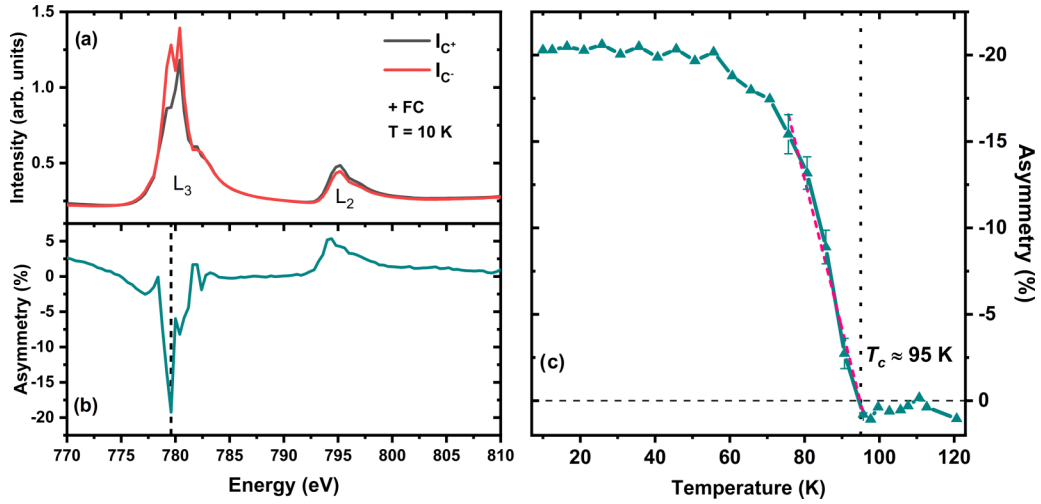


FIG. 4. (a) X-ray reflectivity of Ge-CCO at $T = 10$ K around the Co $L_{2,3}$ edges when field cooled (FC) at 0.2 T, for circular right (C_+) and left (C_-) polarizations. (b) Asymmetry as a function of energy. The dashed line indicates the energy with the largest asymmetry (in absolute values). (c) Magnetic asymmetry as a function of temperature measured at Co L_3 edge [energy of the dashed line in (b)], for a sample FC at 0.2 T. The pink dashed line estimates T_C . The small asymmetry offset above the Curie temperature is presumably due to an imperfect normalization procedure.

dichroism for pure CCO [Figs. 6(a) and 6(b)] and Ge-CCO [Figs. 6(c) and 6(d)] at 779 eV collected at UE46_PGM1 beamline (BEISS II). For pure CCO, both linear and circular dichroism attain their maximum around 0.68 r.l.u. In contrast, Ge-CCO exhibits an extremum for linear dichroism around $q \approx 0.70$ r.l.u. (marked by the green dashed line), while the extremum for circular dichroism is around $q \approx 0.72$ r.l.u. (marked by a blue dashed line). This difference in q for the extrema indicates that the diffraction peak is composed of more than a single magnetic contribution.

B. XMCD on Ge-CCO collected by XEOL

The x-ray intensity transmitted through the film is measured by observing the XEOL signal, and it can be described as

$$I(z) = I_o \Lambda(E) e^{-\mu(E)z}, \quad (2)$$

where z is the thickness, I_o is the incident intensity, μ is the energy-dependent absorption coefficient of the sample, and $\Lambda(E)$ is the energy-dependent efficiency function of XEOL for the substrate used (the typical value for MgO at Co $L_{2,3}$

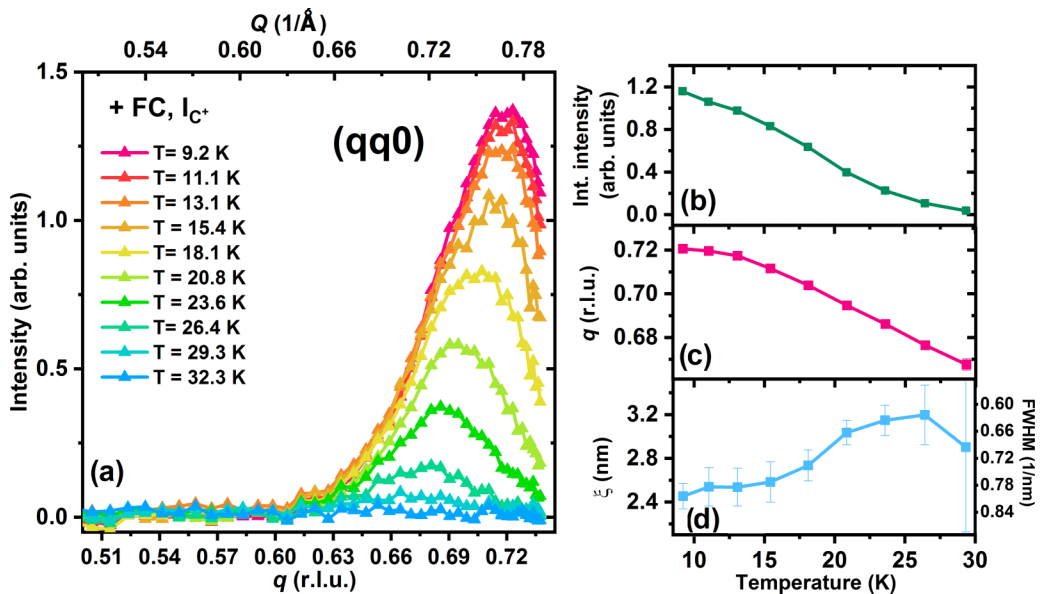


FIG. 5. (a) Temperature dependence of the magnetic diffraction peak ($qq0$) of Ge-CCO upon warming, after field cooling in 0.2 T and using C_+ polarized x rays at 780 eV. The data are presented as a function of both reciprocal lattice units (r.l.u.) (bottom axis) and total momentum transfer (Q) (top axis). (b)–(d) represent the temperature dependence of integrated intensity, modulation parameter q , and the correlation length ξ extracted from the full width at half maximum (FWHM) of data shown in (a).

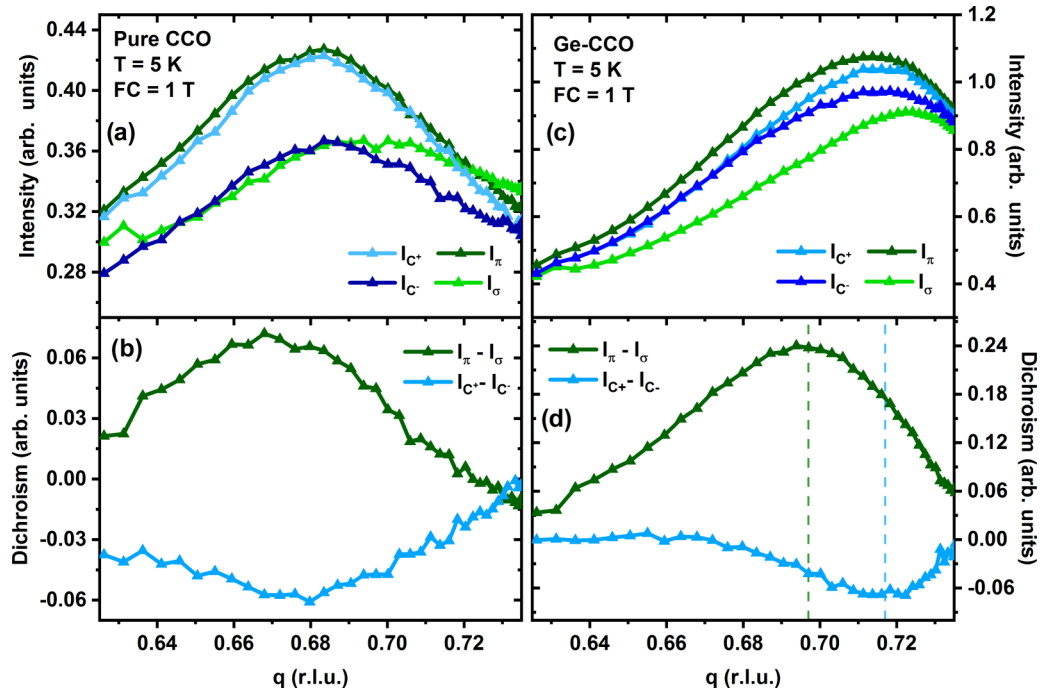


FIG. 6. Magnetic diffraction ($qq0$) peak for circular and linear polarizations with their respective linear and circular dichroism for (a) and (b) CCO and (c) and (d) Ge-CCO. Data collected at 779 eV.

edge is 0.028 [29]). Considering the thickness of the substrate is ≈ 1 mm, we can assume that the entire signal is absorbed by the substrate, and therefore, the entire measured signal is XEOL [29]. Using Eq. (2), we calculate the absorption (μ) from the experimental XEOL data for each helicity of the incident x-ray polarization. Figure 7(a) shows the x-ray absorption spectroscopy (XAS) ($\mu_+ + \mu_-$) and the integrated

XAS after subtracting a two-steplike function (blue line), which accounts for the transitions to the continuum. The helicity of the x ray is indicated by the subscript of the absorption coefficient as μ_{\pm} . Figure 7(b) displays the corresponding XMCD ($\mu_+ - \mu_-$) and its integrated intensity. The XMCD exhibits its maximum at 777.5 eV. Additionally, through the XMCD sum rules analysis [34], the spin (m_s) and orbital (m_l) contributions to the Co^{2+} moment were calculated. We have used $N_h = 3$ as the number of holes in the $3d$ orbital of Co^{2+} . The results obtained are $m_s = -1.3 \pm 0.1 \mu_B/\text{atom}$ and $m_l = -0.36 \pm 0.03 \mu_B/\text{atom}$. These values are, within the uncertainty, equal to those reported by CCO thin films [8].

Furthermore, hysteresis loops were recorded by means of XMCD at 777.5 eV for various temperatures, as shown in Fig. 8. For each applied magnetic field, measurements below the absorption edge (770 eV) have been used for baseline correction. These data show that, for $T \leq 40$ K, a magnetic field of 6.8 T is insufficient to saturate the magnetization, indicative of a very large coercivity and larger saturation field when compared with pure CCO thin film, as reported in Ref. [8].

C. RSXS on Ge-CCO and pure CCO under high magnetic fields

Figure 9 presents the energy dependence of the magnetic diffraction ($qq0$) peak ($q \approx 0.69$) on pure CCO and Ge-CCO for opposite circular polarizations. Both samples have been FC at -6 T from room temperature to 5 K, and a magnetic field of -6 T was applied during the measurements.

The energy dependence of the ($qq0$) reflection at $q = 0.695$ r.l.u. has similar features for both materials, with a maximum at 779 eV and a shoulder around 778.3 eV. However, in the case of pure CCO, the spectrum of the diffraction

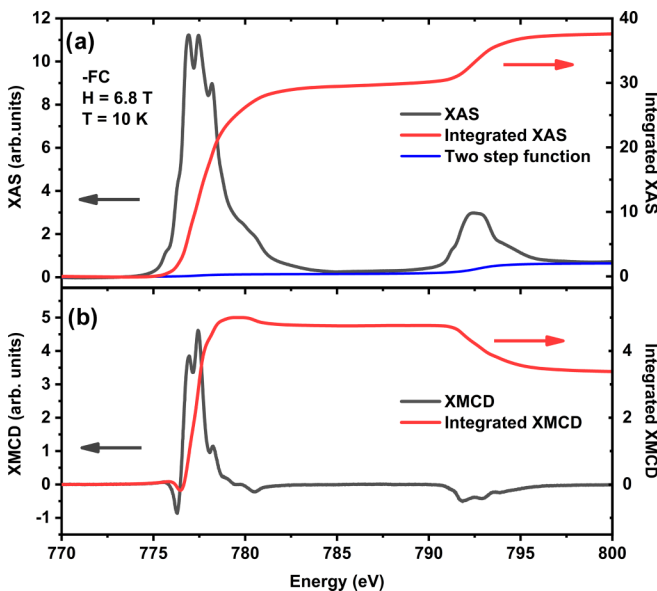


FIG. 7. (a) X-ray absorption spectroscopy (XAS) (black) and integrated XAS (red) of $\text{Co } L_{2,3}$ edge on Ge-CCO collected in x-ray excited optical luminescence (XEOL) mode at 10 K, under 6.8 T and field cooled (FC) at -0.2 T. The integrated XAS has been calculated after removal of the two-steplike function (blue). (b) XMCD data obtained from (a).

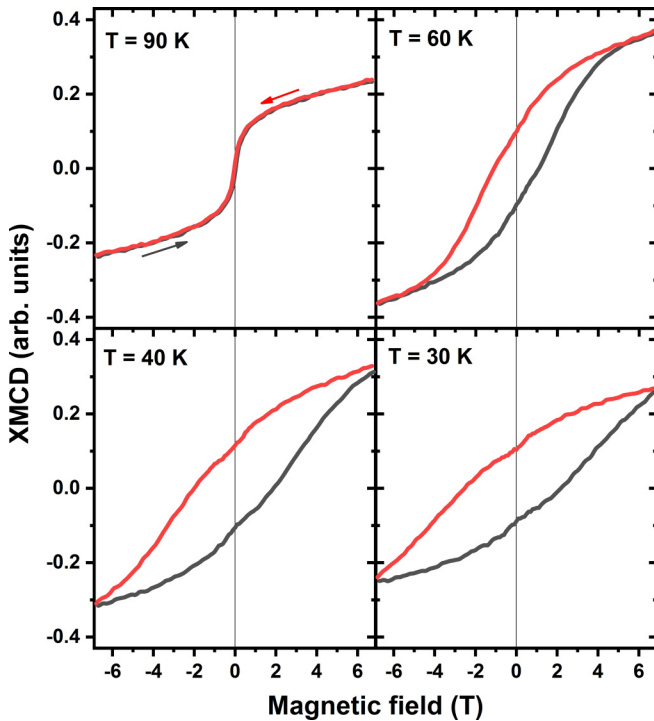


FIG. 8. Magnetic hysteresis loop of Co sublattice in Ge-CCO for various temperatures measured in x-ray excited optical luminescence (XEOL) mode.

peak is broader and less pronounced than in Ge-CCO. The observed circular dichroism in Ge-CCO and pure CCO have opposite signs at 779 eV [Figs. 9(c) and 9(d)].

To learn more about the observed circular dichroism, we studied the field dependence of the $(qq0)$ peak at 779 eV. We collected two datasets with opposite applied fields for each sample. In the first dataset, both materials were cooled under a field of -1 T from 120 to 5 K, and data were acquired while increasing the applied field in several steps from 0 to -6.5 T. For the second dataset, the samples were cooled at 6.5 T from 60 K (which is fully sufficient for reversing the magnetization) to 5 K, and the same procedure was carried out, with the exception that the measurements were done while decreasing the applied field in steps from 6.5 to 0 T.

Figure 10 displays $(qq0)$ peak under various magnetic fields on pure CCO [Fig. 10(a)] and on Ge-CCO [Fig. 10(b)] for the case of negative FC and incident C_+ polarization. The sharp peak observed around $q = 0.71$ r.l.u. is an artifact caused by secondary electrons when the magnetic field points to the detector, as explained previously. The application of the field results mainly in a reduction and/or distortion of the $(qq0)$ reflection intensity for both materials.

The circular dichroism observed in the diffraction peak of a spin spiral defines the sign of the cycloidal rotation of the magnetic moments like those found in TbMnO_3 [35] or DyMnO_3 [36]. From now on, we refer to the circular dichroism of the magnetic diffraction $(qq0)$ peak as helicity contrast, defined as $\frac{I_{c^+} - I_{c^-}}{\int (I_{c^+} + I_{c^-}) dq}$.

In Fig. 11, we present the helicity contrast of the $(qq0)$ peak for the different sets of measurements: for pure CCO with negative [Fig. 11(a)] and positive [Fig. 11(b)] applied

magnetic fields. The case of Ge-CCO is shown in Figs. 11(c) and 11(d) for negative and positive applied magnetic fields, respectively.

While being significantly different in shape, the helicity contrast shows a mirror effect between opposite applied field directions for both materials [Figs. 11(c) and 11(d)]. Therefore, both materials exhibit a direct correlation between the direction of magnetic FC and cycloidal rotation. Insets in Figs. 11(a) and 11(b) show the helicity sense, indicated by the orange arrows. In addition, the helicity contrast decreases for increasing fields for CCO, possibly due to a field-dependent elliptical distortion of the cycloid. The behavior of Ge-CCO, though, is more complex. There are two extrema in the helicity contrast as a function of q . At $q_1 \approx 0.72$ r.l.u., we observe a maximum-minimum for positive-negative applied fields, like pure CCO. The helicity contrast is reduced when the magnetic field increases, irrespective of the magnetic field direction. At a lower q , the extremum around $q_2 \approx 0.68$ r.l.u. is enhanced at larger applied fields. The two extrema q_1 and q_2 show opposite helicity to each other. The sign change in the helicity contrast as a function of q exhibited by Ge-CCO is not observed in pure CCO, which only possesses a single maximum or minimum depending on the sign of the applied field. The observation of two extrema in Ge-CCO may be interpreted as the appearance of a second cycloidal component with slightly smaller q and opposite helicity. To extract field-induced changes, the signal collected under $H = 0$ T has been subtracted from the data collected under field, as shown in Fig. 12. Pure CCO shows a subtle extremum around 0.66 r.l.u., which reflects a small change in the peak shape. In Ge-CCO, however, a single clear maximum around $q = 0.69$ r.l.u. is observed, indicating that the magnetic contribution at q_1 , observed in the zero-field contrast is independent of the applied magnetic field.

IV. DISCUSSION AND CONCLUSIONS

The Ge-doped CCO thin film exhibits magnetic transitions at temperatures like those observed in pure CCO [8], with $T_C \approx 95$ K and the multiferroic phase appearing around $T_S \approx 27$ K. However, the more relevant Ge-doping effect is that defects commonly lead to an increased angular momentum and, correspondingly, to a larger coercive field and a larger anisotropy, as it has been observed in our Ge-CCO thin films. The change in anisotropy could be triggering a different magnetic ground state, as in a frustrated system; a slight unbalancing of the anisotropy term in the Hamiltonian may be sufficient for achieving a magnetic ground state that lies close in energy to the balanced ground state. This increase of the coercive field makes Ge-CCO thin films a potential candidate to study its effect on possible giant magneto-optical effect, as observed in single crystals of CCO [37]. Studying the $(qq0)$ magnetic diffraction peak of Ge-CCO, we observe that q is temperature dependent and goes from a commensurate value of 0.67 r.l.u. values at 27 K to incommensurate 0.72 r.l.u. at 9 K (Fig. 5). These values are larger, at least by 0.03 r.l.u., than the ones reported for the CCO film [8]. Furthermore, an increase in the correlation length is observed with increasing temperature. This is possibly an indication that Ge-CCO undergoes a magnetic phase transition (T_F) around 18 K, like

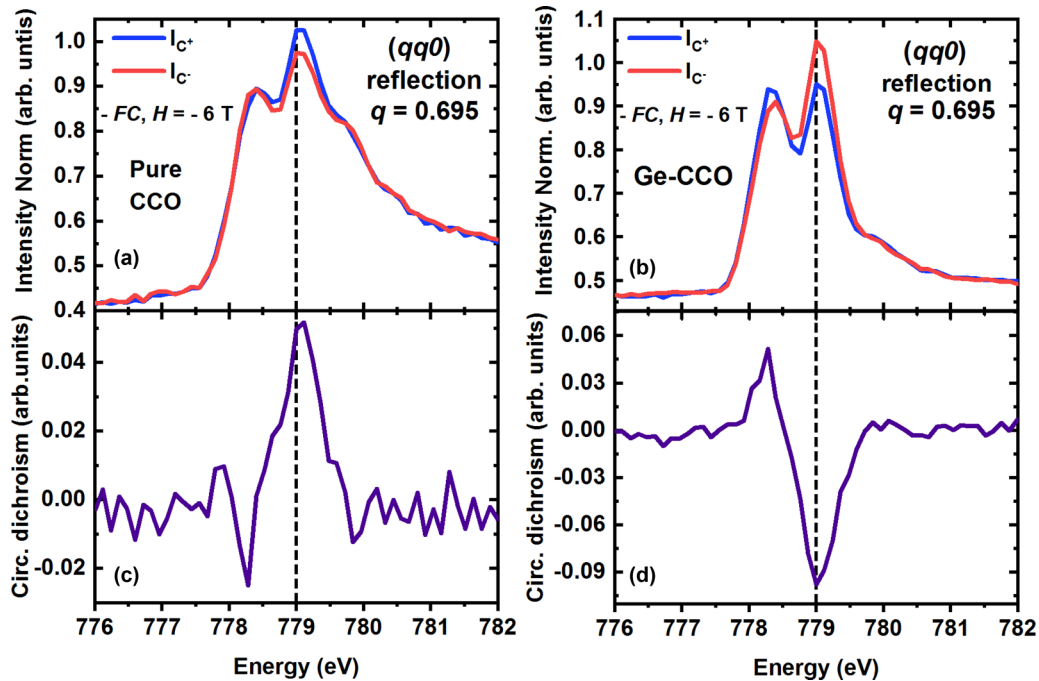


FIG. 9. Energy dependence of the magnetic diffraction ($qq0$) peak for C_+ and C^- polarizations for (a) pure CCO and (b) Ge-CCO at 5 K, under magnetic field applied of -6 T after field cooled (FC) at -6 T. Energy dependence of the circular dichroism of the ($qq0$) peak for (c) pure CCO and (d) Ge-CCO. Dashed lines indicate the energy corresponding to the extrema of circular dichroism.

what has been reported in bulk CCO [4–7] but not observed in pure CCO films. This view is supported by the linear and circular dichroism extrema observed around $q \approx 0.70$ and 0.72 r.l.u. in Ge-CCO (Fig. 6). These observations could be an indication of the coexistence of multiple spin cycloidal textures for temperatures below T_F , as found in bulk CCO [5,6], where the ($qq0$) magnetic peak splits into three different components below T_F .

The multiple spin cycloidal scenario in Ge-CCO gets further support from the results observed in high magnetic field, where a distinct pattern is observed in the helicity contrast

possessing a maximum and a minimum at different values of q (Fig. 11). As the diffraction contrast between circular polarizations relates directly to the sense of the cycloidal rotation, it indicates that the two extrema with opposite signs, at q_1 and q_2 , represent two different modulation vectors close to ($qq0$) with opposite-handed spin rotations. Interestingly, in CCO, the helicity contrast features just one maximum, whose intensity is reduced when magnetic field increases. This may simply reflect a reduction and/or a distortion (ellipticity) of the cone aperture angle (which defines the moment contribution of the cycloid) as the moments try to align with

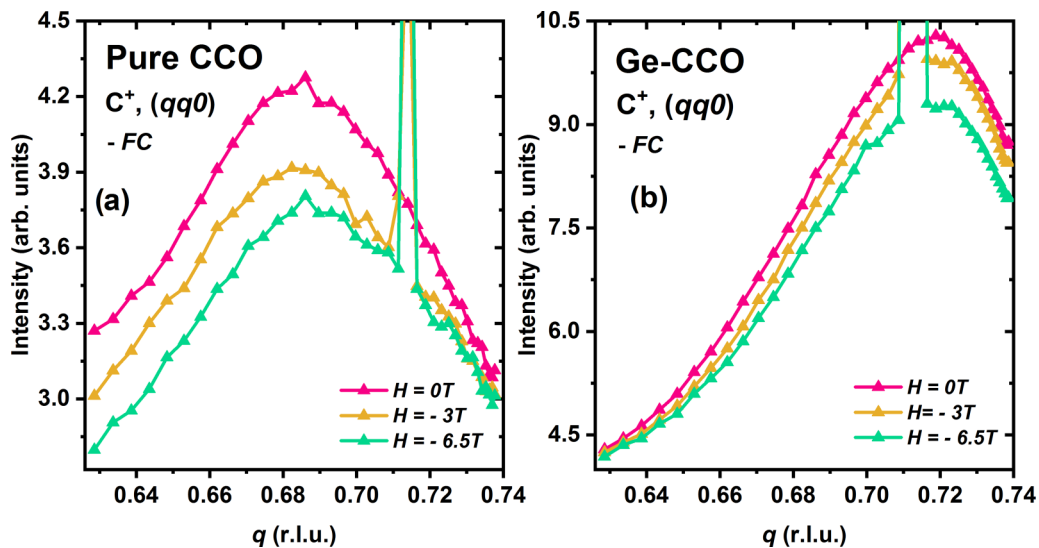


FIG. 10. Intensity of magnetic diffraction peak ($qq0$) of (a) pure CCO and (b) Ge-CCO for various magnetic fields at 779 eV. At 5 K, data collected with C_+ polarized light, field cooled at -1 T. The origin of the artifact around $q \approx 0.712$ is explained in the text.

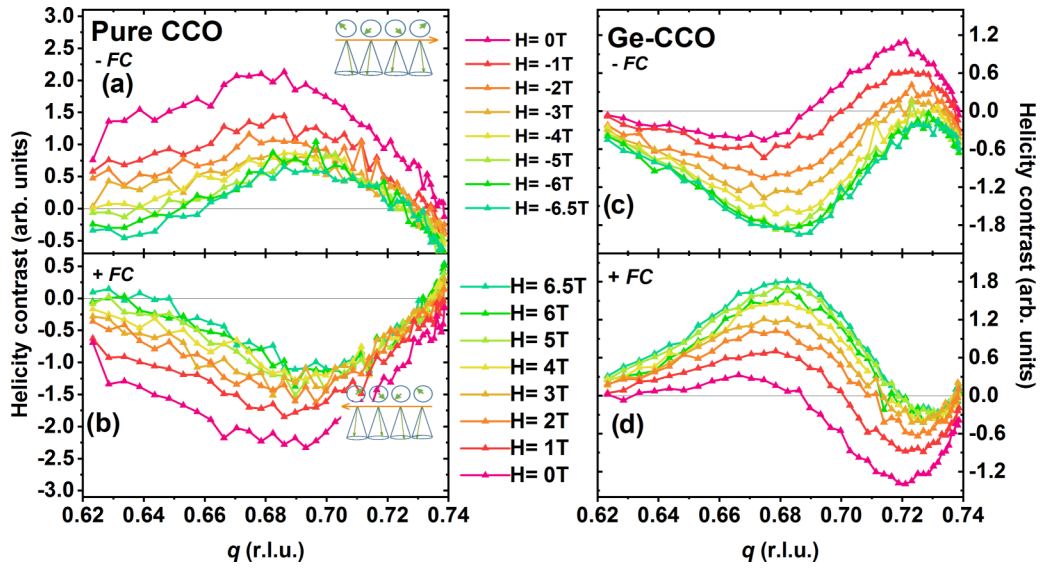


FIG. 11. Helicity contrast of the $(qq0)$ peak for various magnetic fields at 5 K on (a) and (b) pure CCO and (c) and (d) Ge-CCO at 779 eV. (a) and (c) panels are for negative magnetic field cases and (b) and (d) for positive magnetic field cases. Insets in (a) and (b) panels are the sketch of the magnetic modulation vector (orange arrows) and magnetic moments (green arrows). The slight vertical shift between both field cooled (FC) processes for pristine CCO and Ge-CCO is likely to be an experimental artifact, which is in the order of the uncertainty of our experimental data.

the magnetic field. For the case of Ge-CCO, q_1 behaves as CCO, while q_2 gets enhanced with increase in magnetic field. These results show that Ge-CCO has at least two types of spin cycloids oriented differently with respect to each other or having a different length of the propagation vector with different helicity. Assuming the low temperature phase, below T_F , is characterized by the appearance of the commensurate $(\frac{2}{3}, \frac{2}{3}, 0)$ modulation and some satellite reflections, as reported in Refs. [5,6], the satellite at q_1 may be the order parameter of the low temperature phase for Ge-CCO films. The difference in behavior of Ge-CCO and CCO may be because the CCO thin film has much lower $T_F < 5$ K because of the strain,

which makes such a transition observable in bulk but not in the pure CCO films. The difference in T_F between Ge-CCO and CCO implies that Ge doping directly affects the tiny balance between the magnetic exchange interactions, while having negligible effect on the temperature of the ferrimagnetic and multiferroic ordering that are more sensitive to the overall scale of the magnetic exchange constants.

An interesting observation in this paper is a direct correlation between the magnetic FC and the spin cycloidal rotation, shown in Fig. 11. As explained earlier, the circular dichroism of a magnetic diffraction signal relates to the helicity of the cycloidal rotation. According to the relationship of the

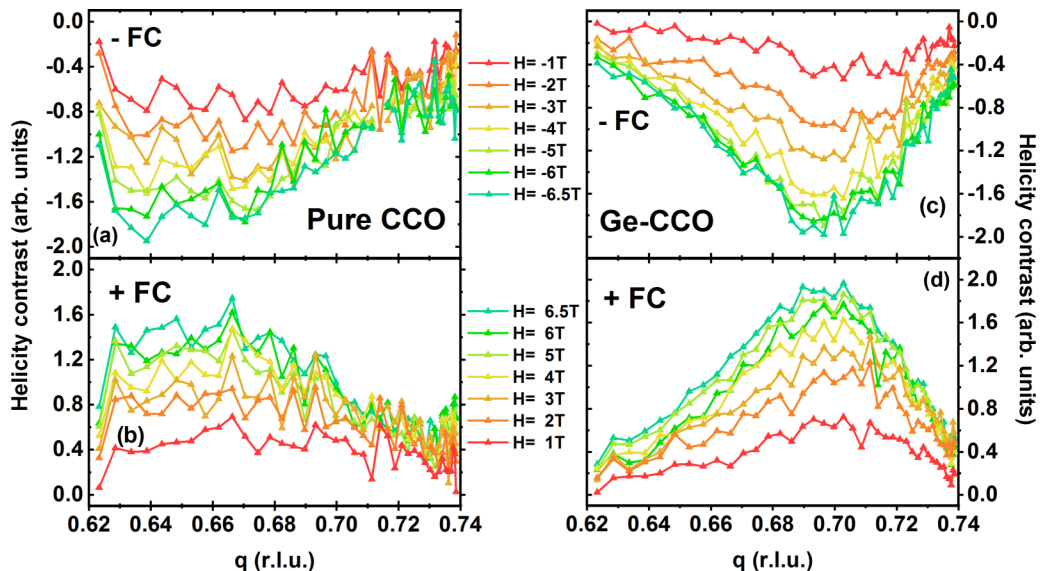


FIG. 12. Helicity contrast of the $(qq0)$ reflection for various magnetic fields after subtracting the zero-field signal. Results of (a) and (b) CCO and (c) and (d) Ge-CCO for negative field cooling (FC) and positive FC, respectively.

electric polarization to the spiral rotation $P \propto e_{ij} (S_i S_j)$ [14] for a thin film, the reversal of the spin cycloidal leads to the reversal of the polarization. Here, we report the reversal of the spin cycloid and, consequently, the reversal of the polarization through only magnetic FC. Usually, in multiferroics, a combination of electric and magnetic fields is needed to achieve a single domain state. For our samples, it is unclear why magnetic FC alone produces a single multiferroic domain state. This may be because the polarization direction in these thin films is well defined without the need for fixing it through an electric FC process or bringing the question to a more basic level: why does the conical state emerge in a single domain without an external stimulus (i.e., electric field)? In general, we can propose a few mechanisms, which lead to a bias that can distinguish between two helicity states. (1) A bias created by the difference of voltage applied before the measurements to charge the sample could define the polarization direction. This scenario is, however, unlikely since the applied voltage produces an electric field perpendicular to the sample surface (the [110] direction) which does not affect the polarization that lies along $[\bar{1}\bar{1}0]$. (2) X rays polarize the sample, as reported by Schierle *et al.* [36], leading to a defined cycloidal rotation domain. This scenario is again not applicable in our case since we observe a reversal of the cycloidal rotation, i.e., reversal in polarization, for opposite magnetic field cooling from above T_C . (3) Bias produced by inversion symmetry breaking due to strain at the interface is another possibility. However, the strain does not break inversion symmetry along the in-plane $[\bar{1}\bar{1}0]$ direction. (4) A plausible explanation could be a bias produced along $[\bar{1}\bar{1}0]$ by antisymmetric exchange, i.e., Dzyaloshinskii-Moriya (DM) interaction. The bias could be a consequence of the broken mirror symmetry due to the surface, producing a weak ferromagnetism caused by canting of all the moments near to the surface toward the normal direction [38]. This canting produces the DM vectors along $[\bar{1}\bar{1}0]$. In this case, inverting the external field may cause the inversion of all DM vectors and, therefore, the distinction between the two helicity states. In any case, further investi-

gations on the origin of this effect is required to confirm such a hypothesis.

In summary, our x-ray investigation finds that Ge doping in CCO does not alter the main magnetic properties in the ferrimagnetic state nor the onset of the multiferroic phase. Despite the similarity in the temperature of phase transitions, the ground state of the Ge-doped film shows a more complex magnetic behavior below T_S than the pure CCO films. We find the occurrence of a second cycloidal component in the magnetic structure, which is close to commensurate, which might represent the phase below $T_F = 15$ K occurring in bulk CCO. Only one of the cycloids observed in the doped system is magnetic field dependent, although surprisingly, both reverse their helicity, which also represents an inversion of the electric polarization, for opposite FC.

Experimental and derived data are accessible from the PSI Public Data Repository [39].

ACKNOWLEDGMENTS

We gratefully thank the X11MA and X07MA beamline staff for experimental support. The financial support of the Swiss National Science Foundation (SNSF) and its National Center of Competence in Research, Molecular Ultrafast Science and Technology (NCCR MUST) Grants No. 51NF40-183615 is acknowledged, and M. Ramakrishnan and N.O.H. acknowledge financial support of the SNSF (Sinergia Projects “Toroidal moments” No. CRSII2_147606 and No. 200021_169017, respectively). H.U. acknowledges financial support from Horizon 2020, the EU Framework Programme for Research and Innovation under the Marie Skłodowska-Curie Grant Agreement No. 801459-FP-RESOMUS and the SNSF through the NCCR MUST. The research leading to this result has been supported by the project CALIPSOplus under the Grant Agreement No. 730872 from Horizon 2020, the EU Framework Programme for Research and Innovation. M. Radovic acknowledges financial support from SNSF under Research Grant No. 200021_182695.

-
- [1] N. A. Spaldin and M. Fiebig, The renaissance of magnetoelectric multiferroics, *Science* **309**, 391 (2005).
 - [2] M. Fiebig, T. Lottermoser, D. Meier, and M. Trassinetti, The evolution of multiferroics, *Nat. Rev. Mater.* **1**, 16046, 2016.
 - [3] N. Menyuk, K. Dwight, and A. Wold, Ferrimagnetic spiral configurations in cobalt chromite, *J. Phys. (Orsay, Fr.)* **25**, 528 (1964).
 - [4] Y. Yamasaki, S. Miyasaka, Y. Kaneko, J. P. He, T. Arima, and Y. Tokura, Magnetic Reversal of the Ferroelectric Polarization in a Multiferroic Spinel Oxide, *Phys. Rev. Lett.* **96**, 207204 (2006).
 - [5] Y. J. Choi, J. Okamoto, D. J. Huang, K. S. Chao, H. J. Lin, C. T. Chen, M. Van Veenendaal, T. A. Kaplan, and S. W. Cheong, Thermally or Magnetically Induced Polarization Reversal in the Multiferroic CoCr_2O_4 , *Phys. Rev. Lett.* **102**, 067601 (2009).
 - [6] L. J. Chang, D. J. Huang, W. H. Li, S. W. Cheong, W. Ratcliff, and J. W. Lynn, Crossover from incommensurate to commensurate magnetic orderings in CoCr_2O_4 , *J. Phys.: Condens. Matter* **21**, 456008 (2009).
 - [7] V. Tsurkan, S. Zherlitsyn, S. Yasin, V. Felea, Y. Skourski, J. Deisenhofer, H. A. Von Nidda, J. Wosnitza, and A. Loidl, Unconventional Magnetostructural Transition in CoCr_2O_4 at High Magnetic Fields, *Phys. Rev. Lett.* **110**, 115502 (2013).
 - [8] Y. W. Windsor, C. Piamonteze, M. Ramakrishnan, A. Scaramucci, L. Rettig, J. A. Huever, E. M. Bothschafter, N. S. Bingham, A. Alberca, S. R. V. Avula, B. Noheda, and U. Staub, Magnetic properties of strained multiferroic CoCr_2O_4 : A soft x-ray study, *Phys. Rev. B* **95**, 224413 (2017).
 - [9] X. Liu, M. Kareev, Y. Cao, J. Liu, S. Middey, D. Meyers, J. W. Freeland, and J. Chakhalian, Electronic and magnetic properties of (111)-oriented CoCr_2O_4 epitaxial thin film, *Appl. Phys. Lett.* **105**, 042401 (2014).
 - [10] R. Guzman, J. Heuver, S. Matzen, C. Magen, and B. Noheda, Structural and magnetic properties of [001] CoCr_2O_4 thin films, *Phys. Rev. B* **96**, 104105 (2017).
 - [11] J. A. Heuver, A. Scaramucci, Y. Blickenstorfer, S. Matzen, N. A. Spaldin, C. Ederer, and B. Noheda, Strain-induced magnetic

- anisotropy in epitaxial thin films of the spinel CoCr_2O_4 , *Phys. Rev. B* **92**, 214429 (2015).
- [12] A. Aqeel, N. Vlietstra, J. A. Heuver, G. E. W. Bauer, B. Noheda, B. J. van Wees, and T. T. M. Palstra, Spin-hall magnetoresistance and spin Seebeck effect in spin-spiral and paramagnetic phases of multiferroic CoCr_2O_4 , *Phys. Rev. B* **92**, 224410 (2015).
- [13] K. Tomiyasu, J. Fukunaga, and H. Suzuki, Magnetic short-range order and reentrant-spin-glass-like behavior in CoCr_2O_4 and MnCr_2O_4 by means of neutron scattering and magnetization measurements, *Phys. Rev. B* **70**, 214434 (2004).
- [14] H. Katsura, N. Nagaosa, and A. V. Balatsky, Spin Current and Magnetoelectric Effect in Noncollinear Magnets, *Phys. Rev. Lett.* **95**, 057205 (2005).
- [15] E. Weschke, H. Ott, E. Schierle, C. Schueß, D. V. Vyalikh, G. Kaindl, V. Leiner, M. Ay, T. Schmitte, H. Zabel, and P. J. Jensen, Finite-Size Effect on Magnetic Ordering Temperatures in Long-Period Antiferromagnets: Holmium Thin Films, *Phys. Rev. Lett.* **93**, 157204 (2004).
- [16] H. Wadati, Okamoto, M. Garganourakis, V. Scagnoli, U. Staub, Y. Yamasaki, H. Nakao, Y. Murakami, M. Mochizuki, M. Nakamura, M. Kawasaki, and Y. Tokura, Origin of the Large Polarization in Multiferroic YMnO_3 Thin Films Revealed by Soft- and Hard-X-Ray Diffraction, *Phys. Rev. Lett.* **108**, 047203 (2012).
- [17] Y. W. Windsor, S. W. Huang, Y. Hu, L. Rettig, A. Alberca, K. Shimamoto, V. Scagnoli, T. Lippert, C. W. Schneider, and U. Staub, Multiferroic Properties of o - LuMnO_3 Controlled by b -Axis Strain, *Phys. Rev. Lett.* **113**, 167202 (2014).
- [18] Y. W. Windsor, M. Ramakrishnan, L. Rettig, A. Alberca, E. M. Bothschafter, U. Staub, K. Shimamoto, Y. Hu, T. Lippert, and C. W. Schneider, Interplay between magnetic order at Mn and Tm sites alongside the structural distortion in multiferroic films of o - TmMnO_3 , *Phys. Rev. B* **91**, 235144 (2015).
- [19] H. Ueda, Y. Tanaka, Y. Wakabayashi, and T. Kimura, Soft x-ray resonant diffraction study of magnetic structure in magnetoelectric Y -type hexaferrite, *Phys. B* **536**, 118 (2018).
- [20] E. Weschke, H. Ott, E. Schierle, C. Schuessler-Langeheine, G. Kaindl, V. Leiner, and H. Zabel, Resonant magnetic x-ray scattering at the lanthanide M_5 edges, *Physica B* **357**, 16 (2005).
- [21] A. J. Hearmon, R. D. Johnson, T. A. W. Beale, S. S. Dhesi, X. Luo, S.-W. Cheong, P. Steadman, and P. G. Radaelli, Magnetic fan structures in $\text{Ba}_{0.5}\text{Sr}_{1.5}\text{Zn}_2\text{Fe}_{12}\text{O}_{22}$ hexaferrite revealed by resonant soft x-ray diffraction, *Phys. Rev. B* **88**, 174413 (2013).
- [22] V. Scagnoli, U. Staub, A. M. Mulders, M. Janousch, G. I. Meijer, G. Hammerl, J. M. Tonnerre, and N. Stojic, Role of magnetic and orbital ordering at the metal-insulator transition in NdNiO_3 , *Phys. Rev. B* **73**, 100409(R) (2006).
- [23] S. B. Wilkins, P. D. Hatton, M. D. Roper, D. Prabhakaran, and A. T. Boothroyd, Soft X-Ray Resonant Magnetic Diffraction, *Phys. Rev. Lett.* **90**, 187201 (2003).
- [24] S. W. Lovesey, E. Balcar, K. S. Knight, and J. Fernández Rodríguez, Electronic properties of crystalline materials observed in x-ray diffraction, *Phys. Rep.* **411**, 233 (2005).
- [25] U. Flechsig, F. Nolting, A. Fraile Rodríguez, J. Krempask, C. Quitmann, T. Schmidt, S. Spielmann, and D. Zimoch, Performance measurements at the SLS SIM beamline, in *SRI 2009, 10th International Conference on Radiation Instrumentation*, edited by R. Garrett, I. Gentle, K. Nugent, and S. Wilkins, AIP Conf. Proc. No. 1234 (AIP, New York, 2010), p. 319.
- [26] U. Staub, V. Scagnoli, Y. Bodenthin, M. García-Fernández, R. Wetter, A. M. Mulders, H. Grimmer, and M. Horisberger, Polarization analysis in soft x-ray diffraction to study magnetic and orbital ordering, *J. Synchrotron Radiat.* **15**, 469 (2008).
- [27] C. Piamonteze, U. Flechsig, S. Rusponi, J. Dreiser, J. Heidler, M. Schmidt, R. Wetter, M. Calvi, T. Schmidt, H. Pruchova, J. Krempasky, C. Quitmann, H. Brune, and F. Nolting, X-Treme beamline at SLS: x-ray magnetic circular and linear dichroism at high field and low temperature, *J. Synchrotron Rad.* **19**, 661 (2012).
- [28] L. Soderholm, G. K. Liu, and M. R. Antonio, X-ray excited optical luminescence (XEOL) detection of x-ray absorption fine structure (XAFS), *J. Chem. Phys.* **109**, 6745 (1998).
- [29] C. Piamonteze, Y. W. Windsor, S. R. V. Avula, E. Kirk, and U. Staub, Soft x-ray absorption of thin films detected using substrate luminescence: a performance analysis, *J. Synchrotron Rad.* **27**, 1289 (2020).
- [30] E. Weschke and E. Schierle, The UE46 PGM-1 beamline at BESSY II, *JLSRF* **4**, A127 (2018).
- [31] J. Fink, E. Schierle, E. Weschke, and J. Geck, Resonant elastic soft x-ray scattering, *Rep. Prog. Phys.* **76**, 056502 (2013).
- [32] J. P. Hannon, G. T. Trammel, M. Blume, D. Gibbs, X-ray Resonance Exchange Scattering, *Phys. Rev. Lett.* **61**, 1245 (1988).
- [33] J. P. Hill and D. F. McMorrow, Resonant exchange scattering: polarization dependence and correlation function, *Acta Cryst. A* **52**, 236 (1996).
- [34] C. T. Chen, Y. U. Idzerda, H. J. Lin, N. V. Smith, G. Meigs, E. Chaban, G. H. Ho, E. Pellegrin, and F. Sette, Experimental Confirmation of the X-Ray Magnetic Circular Dichroism Sum Rules for Iron and Cobalt, *Phys. Rev. Lett.* **75**, 152 (1995).
- [35] H. Jang, J. S. Lee, K. T. Ko, W. S. Noh, T. Y. Koo, J. Y. Kim, K. B. Lee, J. H. Park, C. L. Zhang, S. B. Kim, and S. W. Cheong, Coupled Magnetic Cycloids in Multiferroic TbMnO_3 and $\text{Eu}_{3/4}\text{Y}_{1/4}\text{MnO}_3$, *Phys. Rev. Lett.* **106**, 047203 (2011).
- [36] E. Schierle, V. Soltwisch, D. Schmitz, R. Feyerherm, A. Maljuk, F. Yokaichiya, D. N. Argyriou, and E. Weschke, Cycloidal Order of $4f$ Moments as a Probe of Chiral Domains in DyMnO_3 , *Phys. Rev. Lett.* **105**, 167207 (2010).
- [37] V. Kocsis, S. Bordács, J. Deisenhofer, L. F. Kiss, K. Ohgushi, Y. Kaneko, Y. Tokura, and I. Kézsmárki, Strong magneto-optical effects in ACr_2O_4 ($A = \text{Fe}, \text{Co}$) spinel oxides generated by tetrahedrally coordinated transition metal ions, *Phys. Rev. B* **97**, 125140 (2018).
- [38] F. Hellman *et al.*, Interface-induced phenomena in magnetism, *Rev. Mod. Phys.* **89**, 025006 (2017).
- [39] <https://doi.org/10.16907/c15020ae-6c45-41ba-9131-d0ff87bd7010>.